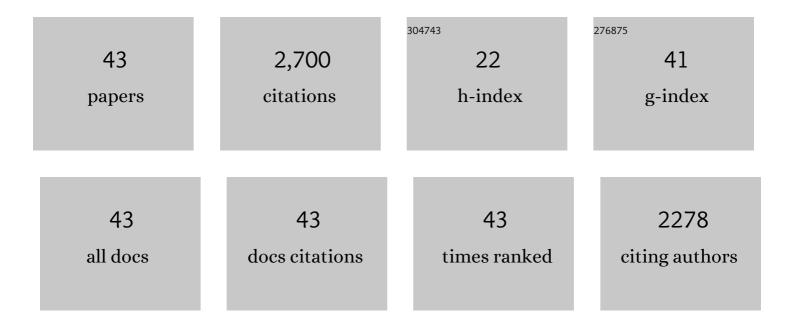
## J Ramon Arrowsmith

List of Publications by Year in descending order

Source: https://exaly.com/author-pdf/8021956/publications.pdf Version: 2024-02-01



#	Article	IF	CITATIONS
1	Uniform California Earthquake Rupture Forecast, Version 3 (UCERF3)The Time-Independent Model. Bulletin of the Seismological Society of America, 2014, 104, 1122-1180.	2.3	424
2	Rapid mapping of ultrafine fault zone topography with structure from motion. , 2014, 10, 969-986.		224
3	Slip in the 1857 and Earlier Large Earthquakes Along the Carrizo Plain, San Andreas Fault. Science, 2010, 327, 1119-1122.	12.6	223
4	Near-Field Deformation from the El Mayor–Cucapah Earthquake Revealed by Differential LIDAR. Science, 2012, 335, 702-705.	12.6	206
5	Tectonic geomorphology of the San Andreas Fault zone from high resolution topography: An example from the Cholame segment. Geomorphology, 2009, 113, 70-81.	2.6	159
6	Fault slip and earthquake recurrence along strike-slip faults — Contributions of high-resolution geomorphic data. Tectonophysics, 2015, 638, 43-62.	2.2	156
7	Late Cenozoic tectonic development of the intramontane Alai Valley, (Pamir-Tien Shan region, central) Tj ETQq1 1 21, 3-1-3-19.	0.784314 2.8	ł rgBT /Over 142
8	High-Resolution Topography-Derived Offsets along the 1857 Fort Tejon Earthquake Rupture Trace, San Andreas Fault. Bulletin of the Seismological Society of America, 2012, 102, 1135-1154.	2.3	98
9	Seismotectonic range-front segmentation and mountain-belt growth in the Pamir-Alai region, Kyrgyzstan (India-Eurasia collision zone). Bulletin of the Geological Society of America, 1999, 111, 1665.	3.3	88
10	Coseismic fault zone deformation revealed with differential lidar: Examples from Japanese <mml:math xmlns:mml="http://www.w3.org/1998/Math/MathML" altimg="si1.gif" overflow="scroll"&gt;<mml:msub><mml:mrow><mml:mi mathvariant="normal"&gt;M</mml:mi </mml:mrow><mml:mrow><mml:mi>w</mml:mi></mml:mrow></mml:msub> intraplate earthquakes. Earth and Planetary Science Letters, 2014, 405, 244-256.</mml:math 	4.4 • <td>83 ath&gt;â^1⁄47</td>	83 ath>â^1⁄47
11	Orogenic-wedge deformation and potential for great earthquakes in the central Andean backarc. Nature Geoscience, 2011, 4, 380-383.	12.9	77
12	The <i>M</i> 7 2016 Kumamoto, Japan, Earthquake: 3â€D Deformation Along the Fault and Within the Damage Zone Constrained From Differential Lidar Topography. Journal of Geophysical Research: Solid Earth, 2018, 123, 6138-6155.	3.4	75
13	Threeâ€dimensional surface displacements and rotations from differencing pre―and postâ€earthquake LiDAR point clouds. Geophysical Research Letters, 2012, 39, .	4.0	73
14	Differential structural and geomorphic mountain-front evolution in an active continental collision zone: The northwest Pamir, southern Kyrgyzstan. Bulletin of the Geological Society of America, 2003, 115, 166-181.	3.3	57
15	Century-long average time intervals between earthquake ruptures of the San Andreas fault in the Carrizo Plain, California. Geology, 2010, 38, 787-790.	4.4	56
16	Climate-Modulated Channel Incision and Rupture History of the San Andreas Fault in the Carrizo Plain. Science, 2010, 327, 1117-1119.	12.6	53
17	Characterization of slow slip rate faults in humid areas: Cimandiri fault zone, Indonesia. Journal of Geophysical Research F: Earth Surface, 2016, 121, 2287-2308.	2.8	53
18	Optimization of legacy lidar data sets for measuring nearâ€field earthquake displacements. Geophysical Research Letters, 2014, 41, 3494-3501	4.0	47

IF

CITATIONS

	Early human impacts and ecosystem reorganization in southern-central Africa. Science Advances, 2021,		
19	7, .	10.3	38
20	Illuminating Northern California's Active Faults. Eos, 2009, 90, 55-55.	0.1	37
21	Surface rupture of the 1911 Kebin (Chon–Kemin) earthquake, Northern Tien Shan, Kyrgyzstan. Geological Society Special Publication, 2017, 432, 233-253.	1.3	35
22	Airborne Lidar and Electro-Optical Imagery along Surface Ruptures of the 2019 Ridgecrest Earthquake Sequence, Southern California. Seismological Research Letters, 2020, 91, 2096-2107.	1.9	31
23	The 2016 M7 Kumamoto, Japan, Earthquake Slip Field Derived From a Joint Inversion of Differential Lidar Topography, Optical Correlation, and InSAR Surface Displacements. Geophysical Research Letters, 2019, 46, 6341-6351.	4.0	30
24	Fault Pattern and Seismotectonic Style of the Campania – Lucania 1980 Earthquake (Mw 6.9, Southern) Tj ET	Qq0 0 0 rg	;BT_/Overlo 24
25	High-resolution surface faulting from the 1983 Idaho Lost River Fault Mw 6.9 earthquake and previous events. Scientific Data, 2021, 8, 68.	5.3	23
26	High-Detail Fault Segmentation: Deep Insight into the Anatomy of the 1983 Borah Peak Earthquake Rupture Zone (Mw 6.9, Idaho, USA). Lithosphere, 2022, 2022, .	1.4	19
27	Revised dates of large earthquakes along the Carrizo section of the San Andreas Fault, California, since A.D. 1310 ± 30. Journal of Geophysical Research, 2009, 114, .	3.3	18
28	The Age and Origin of Small Offsets at Van Matre Ranch along the San Andreas Fault in the Carrizo Plain, California. Bulletin of the Seismological Society of America, 2018, 108, 639-653.	2.3	18
29	Distribution of Aseismic Deformation Along the Central San Andreas and Calaveras Faults From Differencing Repeat Airborne Lidar. Geophysical Research Letters, 2020, 47, e2020GL090628.	4.0	14
30	Volcano morphology as an indicator of stress orientation in the Java Volcanic Arc, Indonesia. Journal of Volcanology and Geothermal Research, 2020, 400, 106912.	2.1	14
31	Reconstructing the Environmental Context of Human Origins in Eastern Africa Through Scientific Drilling. Annual Review of Earth and Planetary Sciences, 2022, 50, 451-476.	11.0	13
32	Neotectonic Activity in the Low-Strain Broken Foreland (Santa Bárbara System) of the North-Western Argentinean Andes (26°S). Lithosphere, 2020, 2020, .	1.4	11
33	Paleoseismic Record of Three Holocene Earthquakes Rupturing the Issykâ€Ata Fault near Bishkek, North Kyrgyzstan. Bulletin of the Seismological Society of America, 2017, 107, 2721-2737.	2.3	10
34	Zero to a trillion: Advancing Earth surface process studies with open access to high-resolution topography. Developments in Earth Surface Processes, 2020, 23, 317-338.	2.8	10
35	Extent of Lowâ€Angle Normal Slip in the 2010 El Mayorâ€Cucapah (Mexico) Earthquake From Differential Lidar. Journal of Geophysical Research: Solid Earth, 2019, 124, 943-956.	3.4	9
36	Reproducibility of San Andreas Fault Slip Rate Measurements at Wallace Creek in the Carrizo Plain, CA. Earth and Space Science, 2019, 6, 156-165.	2.6	8

ARTICLE

#

#	Article	IF	CITATIONS
37	Measuring change at Earth's surface: On-demand vertical and three-dimensional topographic differencing implemented in OpenTopography. , 2021, 17, 1318-1332.		8
38	Differentiating simple and composite tectonic landscapes using numerical fault slip modeling with an example from the south central Alborz Mountains, Iran. Journal of Geophysical Research F: Earth Surface, 2013, 118, 1792-1805.	2.8	7
39	Evidence for Multiple Groundâ€Rupturing Earthquakes in the Past 4,000ÂYears Along the Pasuruan Fault, East Java, Indonesia: Documentation of Active Normal Faulting in the Javan Backarc. Tectonics, 2019, 38, 1489-1506.	2.8	7
40	Late Quaternary Tectonics along the Peri-Adriatic Sector of the Apenninic Chain (Central-Southern) Tj ETQq0 0 C Lithosphere, 2021, 2021, .	) rgBT /Ov 1.4	erlock 10 Tf 5 6
41	The Pamir Frontal Thrust Fault: Holocene Fullâ€Segment Ruptures and Implications for Complex Segment Interactions in a Continental Collision Zone. Journal of Geophysical Research: Solid Earth, 2021, 126, e2021JB022405.	3.4	6
42	Statewide USGS 3DEP Lidar Topographic Differencing Applied to Indiana, USA. Remote Sensing, 2022, 14, 847.	4.0	6
43	Spatiotemporal Rates of Tectonic Deformation and Landscape Evolution above a Laterally Propagating Thrust Fault: Wheeler Ridge Anticline, California, USA. Lithosphere, 2021, 2021, .	1.4	4